

Article

Decomposition of d- and f-Shell Contributions to Uranium Bonding from the Quantum Theory of Atoms in Molecules: Application to Uranium and Uranyl Halides

Jonathan Tanti ^{1,2} , Meghan Lincoln ¹  and Andy Kerridge ^{1,*} ¹ Department of Chemistry, Lancaster University, Lancaster LA1 4YB, UK;

jonathan.tanti@postgrad.manchester.ac.uk (J.T.); meghanlincoln@hotmail.com (M.L.)

² School of Chemistry, The University of Manchester, Oxford Road, Manchester M13 9PL, UK

* Correspondence: a.kerridge@lancaster.ac.uk; Tel.: +44-1-524-594-770

Received: 7 August 2018; Accepted: 20 August 2018; Published: 30 August 2018



Abstract: The electronic structures of a series of uranium hexahalide and uranyl tetrahalide complexes were simulated at the density functional theoretical (DFT) level. The resulting electronic structures were analyzed using a novel application of the Quantum Theory of Atoms in Molecules (QTAIM) by exploiting the high symmetry of the complexes to determine 5f- and 6d-shell contributions to bonding via symmetry arguments. This analysis revealed fluoride ligation to result in strong bonds with a significant covalent character while ligation by chloride and bromide species resulted in more ionic interactions with little differentiation between the ligands. Fluoride ligands were also found to be most capable of perturbing an existing electronic structure. 5f contributions to overlap-driven covalency were found to be larger than 6d contributions for all interactions in all complexes studied while degeneracy-driven covalent contributions showed significantly greater variation. σ -contributions to degeneracy-driven covalency were found to be consistently larger than those of individual π -components while the total π -contribution was, in some cases, larger. Strong correlations were found between overlap-driven covalent bond contributions, U–O vibrational frequencies, and energetic stability, which indicates that overlap-driven covalency leads to bond stabilization in these complexes and that uranyl vibrational frequencies can be used to quantitatively probe equatorial bond covalency. For uranium hexahalides, degeneracy-driven covalency was found to anti-correlate with bond stability.

Keywords: uranium; uranyl; halide; covalency; QTAIM; CASSCF; DFT; electron density

1. Introduction

The quantification of the covalent contribution to bonding in complexes of the f-elements is an area of great current research being explored via X-ray absorption [1–11], electron paramagnetic [12–15], nuclear magnetic resonance [16,17], emission [18,19], and photoelectron [20] spectroscopies as well as X-ray diffraction [21] and structural studies [22–30]. The latter have often been carried out in combination with theoretical studies and a wealth of purely theoretical data also exists [31–53]. However, covalency is a phenomenon that is open to significant interpretation. It can manifest due to (i) the near-degeneracy of energy levels and/or (ii) the spatial overlap of the electronic wave functions of interacting species and, of these, only the latter leads to the accumulation of electronic charge in the bonding region and, therefore, the potential for energetic stabilization of the bond. Differentiating between these two origins of covalent bond character is, in addition to being of fundamental interest, of significant practical importance. Current European [54] and US [55] strategies for the separation of

trivalent lanthanides from the highly radioactive minor actinides (Np, Am, and Cm) in spent nuclear fuel are based on the exploitation of energetic stabilization of complexes of the latter with the origin of this stability believed to be due to the greater chemical availability of the 5f valence shell.

Recently, several groups have adopted Bader's Quantum Theory of Atoms in Molecules (QTAIM) [56] in order to probe covalency from a computational perspective. The QTAIM has the capacity to differentiate between degeneracy-driven and overlap-driven contributions to bonding interactions [57]. It is an appealing method of analysis since its results are independent of the orbital basis used to express the electronic structure, which cannot be unambiguously defined. This characteristic means that the QTAIM is equally applicable to electronic structures obtained using any quantum chemical methodology and, since it analyzes the physically observable electron density, it can be applied to experimentally-determined data [21,58].

Complexes of the f-elements typically exhibit strong relativistic effects, substantial dynamical electron correlation, and weak crystal fields and these factors combine to produce electronic structures in which the 5f, 6d, and, to a lesser extent, the 7s valence shells exist at similar energies, which complicates the role that these shells play in covalent interactions. Recently, we have shown that the QTAIM can be exploited in systems of high symmetry to differentiate between the roles played by the 5f and 6d shells [59–61]. In this study, we further extend this approach to distinguish between σ -components and π -components of covalent bond character. This approach is applied to a series of homo-halide and hetero-halide complexes of the general form $[\text{UO}_2\text{X}_2\text{Y}_2]^{2-}$ and $\text{UX}_2\text{Y}_2\text{Z}_2$ where X, Y, Z \in {F, Cl, Br}. These complexes have been selected due to their high symmetry (D_{2h} or higher) when assuming a *trans* orientation of like ligands and because they include a number of synthetically realized species: $[\text{UCl}_6]^{2-}$ and $[\text{UF}_6]^-$ have both been the subject of recent experimental studies of U–X bonding [5,21] while the experimentally determined electronic structure of $\text{Cs}_2\text{UO}_2\text{Cl}_4$ has been previously analyzed using the QTAIM [58]. Of the remaining complexes, $[\text{UO}_2\text{F}_4]^{2-}$ and $[\text{UO}_2\text{Br}_4]^{2-}$ have been observed in the gas and condensed phases, respectively [62,63]. $[\text{UF}_6]^-$ and $[\text{UCl}_6]^-$ have both been experimentally characterized [64–66] although $[\text{UBr}_6]^-$ remains unreported.

2. Results

2.1. Identification of Model Chemistry

The performance of a number of *xc*-functionals was assessed in order to determine the most suitable model chemistry for the study. The functionals chosen for this exercise were the GGA functionals PBE [67] and BLYP [68,69] along with the hybrid-GGA functionals PBE0 [70], B3LYP [71,72], and BHLYP [73]. A variation of the chosen basis set was not considered since its large size was assumed to give results sufficiently close to the basis set limit. Additionally, it has recently been shown that the def2-QZVP basis set used for the ligand ions is sufficient for modeling anions in the absence of diffuse functions [74]. For these test calculations, two representative systems were considered: $[\text{UO}_2\text{Cl}_4]^{2-}$ and UF_6 , for which accurate experimental data exists.

Tables 1 and 2 summarize selected structural and vibrational parameters of these systems. In particular, only frequencies of vibrational stretching modes are reported since these most clearly relate to bond strength. As expected, hybrid functionals tend to outperform pure GGA functionals. Of the hybrid functionals, BHLYP (incorporating 50% Hartree-Fock exchange) is outperformed by both B3LYP and PBE0 (incorporating 20% and 25% Hartree-Fock exchange, respectively) especially with respect to vibrational frequencies. B3LYP and PBE0 perform comparably well and are in good to excellent agreement with experimental parameters. B3LYP noticeably outperforms PBE0 in the simulation of U–O bond lengths and vibrational frequencies in $[\text{UO}_2\text{Cl}_4]^{2-}$ and was chosen as the *xc*-functional used in the remainder of this study. The accuracy of the B3LYP functional reported in this study is comparable to that previously reported for other simple uranyl coordination complexes [75] and for f-element hexachlorides (M = U, Ce) [61].

Table 1. Calculated structural and vibrational parameters of $[\text{UO}_2\text{Cl}_4]^{2-}$ calculated with various exchange-correlation functionals. Values in parenthesis indicate deviations from experimental values. ^a ref [76], ^b ref. [77].

Parameter	Exp. ^{a,b}	BLYP	PBE	PBE0	B3LYP	BHLYP
r_{UO} (Å)	1.774	1.817 (+0.043)	1.800 (+0.026)	1.756 (−0.018)	1.776 (+0.002)	1.735 (−0.039)
r_{UCl} (Å)	2.671	2.765 (+0.094)	2.721 (+0.050)	2.715 (+0.044)	2.749 (+0.078)	2.749 (+0.078)
ν_{UO} (cm^{-1})	834	776 (−58)	803 (−31)	896 (+62)	855 (+21)	953 (+119)
	922	862 (−60)	887 (−35)	975 (+53)	939 (+17)	1023 (+101)
ν_{UCl} (cm^{-1})	206	179 (−27)	192 (−14)	199 (−7)	188 (−18)	196 (−10)
	236	197 (39)	238 (+2)	216 (−20)	206 (−30)	213 (−23)
	267	213 (−54)	226 (−41)	234 (−33)	224 (−43)	232 (−25)

Table 2. Calculated structural and vibrational parameters of UF_6 calculated with various exchange-correlation functionals. Values in parenthesis indicate deviations from experimental values. ^a ref [64], ^b ref. [65].

Parameter	Exp. ^{a,b}	BLYP	PBE	PBE0	B3LYP	BHLYP
r_{UF} (Å)	1.999	2.036 (+0.037)	2.018 (+0.019)	1.990 (−0.009)	2.009 (+0.010)	1.984 (−0.055)
ν_{UF} (cm^{-1})	534	511 (−23)	521 (−13)	543 (+9)	532 (−2)	548 (+14)
	626	581 (−45)	596 (−30)	633 (+7)	615 (−11)	648 (+22)
	667	613 (−54)	630 (−37)	682 (+15)	660 (+7)	710 (+43)

2.2. Homohalide Complexes of Uranium and Uranyl

In this section, the simulation and analysis of complexes of the form $[\text{UO}_2\text{X}_4]^{2-}$ and UX_6 ($\text{X} = \text{F}, \text{Cl}, \text{Br}$) is considered. Focusing initially on the uranyl complexes, Table 3 summarizes structural parameters obtained using the B3LYP *xc*-functional.

A clear trend of increasing equatorial bond length is found as the halide mass increases, which is expected with the increasing size of the ligand. There is also, however, a commensurate reduction in the axial U–O bond length, which suggests a weakening of the equatorial bonds. Although equatorial bond lengths are found to be greater than the sum of the ionic radii, the difference is least pronounced for $\text{X} = \text{F}$, which again increases as the halide mass increases. This suggests some degree of covalent bond stabilization for the lighter halides.

As with $[\text{UO}_2\text{Cl}_4]^{2-}$ (Table 1), the U–O bond length in $[\text{UO}_2\text{Br}_4]^{2-}$ is in excellent agreement with the experimentally reported value of 1.766 Å [63]. However, it should be noted that the experimental data are derived from XRD studies of condensed-phase structures. No experimentally determined structural data is available for $[\text{UO}_2\text{F}_4]^{2-}$, which has only been observed in the gas phase [62]. However, the U–O bond length reported here lies between the computationally-derived gas-phase literature values of 1.808 and 1.851 Å obtained using PBE and CCSD(T), respectively, [62] and compares well to that previously obtained using the B3LYP functional [37,78].

Table 3. B3LYP-calculated structural parameters $[\text{UO}_2\text{X}_4]^{2-}$. R = 6-coordinated Shannon ionic radius.

Complex	r_{UO} (Å)	r_{UX} (Å)	$R = R_{\text{U}} + R_{\text{X}}$ (Å)	$r_{\text{UX}} - R$ (Å)
$[\text{UO}_2\text{F}_4]^{2-}$	1.824	2.229	$0.73 + 1.33 = 2.06$	0.169
$[\text{UO}_2\text{Cl}_4]^{2-}$	1.776	2.749	$0.73 + 1.81 = 2.54$	0.209
$[\text{UO}_2\text{Br}_4]^{2-}$	1.769	2.922	$0.73 + 1.96 = 2.69$	0.232
UO_2^{2+}	1.695	-	-	-

The U–Cl bond length is overestimated by 0.078 Å but is identical to that reported previously using the same functional [37] and the U–Br bond length is overestimated by 0.108 Å. The U–F bond length of 2.229 Å is very similar to that reported from PBE (2.233 Å), B3LYP (2.231 Å), and CCSD(T) (2.232 Å) simulations [37,62]. The excellent agreement with the CCSD(T) data, in particular, indicates that the origin of the discrepancies between experimental and calculated values for the chloride and bromide complexes is due to crystal packing effects.

The calculated structural data for UX_6 (Table 4) presents a less clear picture. While the U–X bond lengths again increase as the halides mass increases, a comparison with the sum of ionic radii gives no trend. In contrast to the uranyl halides, bond lengths in these species are shorter than the sum of the ionic radii due to the lack of competition with strongly coordinating terminal oxo ligands. However, this shortening is identical in the fluoride and bromide complexes and less than that found in UCl_6 . The good agreement with the experimental gas-phase U–F bond length (Table 2) is apparently not replicated in UCl_6 where the U–Cl bond is overestimated by 0.050 Å in comparison to the value of 2.42 Å reported experimentally [66]. However, this value is again derived from an XRD study of a condensed-phase structure and so the discrepancy is comparable to those found for $[\text{UO}_2\text{Cl}_4]^{2-}$ and $[\text{UO}_2\text{Br}_4]^{2-}$. The calculated U–Cl bond length is in excellent agreement with that calculated by Batista et al. (2.472 Å) using the same *xc*-functional [79]. There are no experimentally reported simple bromides of uranium [80], but the value reported in this study is in good agreement with and slightly shorter than those reported from GGA-based simulations (2.650–2.687 Å) [81], commensurate with the data presented in Tables 1 and 2. The good agreement with available literature data, therefore, leads us to tentatively suggest that an interplay of electronic and steric effects serve to mask any simple trend in UX_6 bond lengths when compared to ionic radii.

Table 4. B3LYP-calculated structural parameters UX_6 . R = 6-coordinated Shannon ionic radius.

Complex	r_{UX} (Å)	$R = R_{\text{U}} + R_{\text{X}}$ (Å)	$r_{\text{UX}} - R$ (Å)
UF_6	2.009	$0.73 + 1.33 = 2.06$	−0.051
UCl_6	2.470	$0.73 + 1.81 = 2.54$	−0.070
UBr_6	2.639	$0.73 + 1.96 = 2.69$	−0.051

Bonding analysis of these complexes was performed using the Quantum Theory of Atoms In Molecules (QTAIM) [56]. We have recently discussed the merits of this methodology in analyzing the electronic structure of *f*-element complexes [57]. In this study, advantage is taken of the high symmetry of these complexes in order to perform a novel decomposition of a bonding contribution to 5*f* and 6*d* uranium valence shells.

Two QTAIM metrics are commonly used to characterize bonding in molecular systems. The first of these is $\rho_{\text{BCP}}(A, B)$, which is the magnitude of the electronic density at the bond critical point (BCP) between atoms A and B where the BCP is the saddle point in the electronic density distribution $\rho(\mathbf{r})$ being a local maximum on the interatomic surface and a local minimum perpendicular to the surface. A commonly employed rule of thumb is that covalent interactions are characterized by $\rho_{\text{BCP}} > 0.2$ a.u. and closed shell interactions by $\rho_{\text{BCP}} < 0.1$ a.u. with intermediate values indicating an increasing degree of a covalent character. ρ_{BCP} can, therefore, be interpreted as a measure of covalent interaction manifested by orbital overlap.

The second QTAIM metric used to characterize bonding is the delocalization index, $\delta(A, B)$. The delocalization index is an integrated property and, for chemical systems described by a single electronic configuration, can be defined by the equation below:

$$\delta(A, B) = 2 \sum_{i,j} S_{ij}(A)S_{ij}(B) \quad (1)$$

where $S_{ij}(X)$ is the overlap between molecular orbitals (MOs) $\varphi_i(\mathbf{r})$ and $\varphi_j(\mathbf{r})$ integrated over the atomic basin associated with atom X (as defined by QTAIM). $\delta(A, B)$ is a measure of the number of electrons shared between two atoms and, in the absence of bond polarisation, correlates strongly with a formal bond order. More generally, $\delta(A, B)$ can be interpreted as indicating the degree of covalent interaction manifested by energetic degeneracy since it can be large in the absence of significant overlap between species. While, typically, large values of $\rho_{\text{BCP}}(A, B)$ are accompanied by large values of $\delta(A, B)$, the converse is not universally true.

The complexes considered in this study all possess D_{2h} (or higher) symmetry. Since the systems are closed shell in nature, the electron density possesses the same symmetry as the complex it describes and, therefore, the atomic basin associated with the central uranium atom also possesses this symmetry (see Figure 1). The delocalization index between the uranium center and any other atom in the complex can then be decomposed by the equation below.

$$\delta(U, B) = 2 \sum_{\Gamma} \sum_{i,j} S_{ij}(U)S_{ij}(B) \quad (2)$$

where Γ indexes the irreducible representations (irreps) of the point group and the summation over MOs is now limited to those orbitals spanning the irrep Γ . This definition is valid since the overlap integral $S_{ij}(U)$ is only non-zero when the MOs $\varphi_i(\mathbf{r})$ and $\varphi_j(\mathbf{r})$ span the same irreducible representation. We have used a similar, though less developed, approach in considering the contributions to bonding in a series of actinocenes [60].

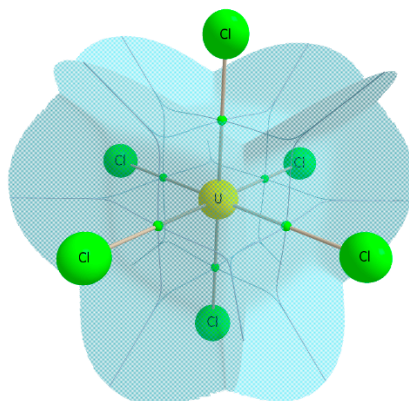


Figure 1. QTAIM derived an atomic basin of U in UCl_6 , which exhibits the full symmetry of the molecule. Figures reproduced from Reference [61].

Table 5. Irreducible representations spanned by components of the 5f and 6d valence shells with respect to the principal molecular axis.

Irrep (Γ)	A_g	B_{1g}	B_{2g}	B_{3g}	A_u	B_{1u}	B_{2u}	B_{3u}
Component	$6d_{\sigma}, 6d_{\delta}$	$6d_{\delta}$	$6d_{\pi}$	$6d_{\pi}$	$5f_{\delta}$	$5f_{\sigma}, 5f_{\delta}$	$5f_{\pi}, 5f_{\phi}$	$5f_{\pi}, 5f_{\phi}$

In D_{2h} symmetry, the components of the 5f and 6d valence shells that can engage in σ -bonding, π -bonding, δ -bonding, and φ -bonding interactions with ligands lying on the principal axis are summarized in Table 5. In the systems under consideration here, δ -bonding and φ -bonding interactions are not possible (or are, at least, energetically highly unfavorable) and σ -bonding and π -bonding contributions from the 5f and 6d shell can be decomposed from the total delocalization index. Similarly, ρ_{BCP} can be decomposed into contributions from the 5f and 6d shells even though further decomposition is not possible since only the σ -bonding contribution is non-zero at the BCP (all other contributions to $\rho(\mathbf{r})$ contain a nodal plane passing through the BCP). Lastly, it should be noted that, even though this decomposition is only valid with respect to bonding contributions aligned with the principal axis of the molecule, in all complexes considered here, the principal axis can be chosen to align with any U–O or U–X bond while maintaining D_{2h} symmetry and, therefore, the decomposition can be applied to all bonding interactions.

Figure 2 summarizes the relevant QTAIM metrics for the U–O bond in $[\text{UO}_2\text{X}_4]^{2-}$ complexes (see Supplementary Materials for numerical data). The magnitude of ρ_{BCP} deviates most strongly from that of free uranyl in the case of the fluoride complex, which is indicative of a weakening of the covalent character of the U–O interaction. As the halide mass increases, so does ρ_{BCP} , which implies that the heavier halides perturb the U–O bond to a lesser extent. This is commensurate with the data presented in Table 3 where covalent stabilization of the equatorial bonds appears most pronounced for the fluoride complex. The values of ρ_{BCP} reported in this study compare well to those previously reported for the fluoride and chloride complexes as well as for the free uranyl ion [37].

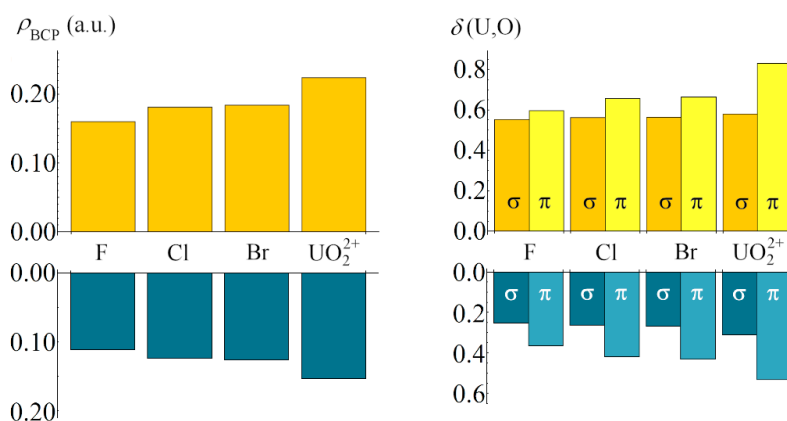


Figure 2. Decomposed QTAIM metrics of the U–O bond in $[\text{UO}_2\text{X}_4]^{2-}$ complexes ($X = \text{F}, \text{Cl}, \text{Br}$) obtained from B3LYP-derived densities. Values from free uranyl are also provided for comparison. f-shell contributions are given in yellow and d-shell contributions are given in blue.

The 5f contribution to ρ_{BCP} accounts for ~60% of the total value irrespective of the species under consideration, which indicates that the 5f-shell is more involved in covalent interactions with the oxo ligand than the 6d-shell. The percentage variations in the 5f and 6d contributions to ρ_{BCP} are extremely similar with values in the fluoride complex being 71% and 73% of the free uranyl values, respectively.

The corresponding $\delta(U,O)$ data demonstrate broadly the same trend, but provide further insight. The total number of electrons shared is substantially lower in the halide complexes than in free uranyl in agreement with previous work [37], but again increases as the halide mass increases and the perturbation of the U–O bond is reduced. $\delta(U,O)$ is 78% of the free uranyl value in the fluoride complex but the 5f contribution accounts for 65% of the total, which is greater than the 63% contribution in free uranyl and indicates a stability of this contribution to the U–O bond with respect to that of free uranyl. The ratio of 5f/6d contributions is reasonably constant across the halides. For example, the 5f component is 64% of the total value in the bromide complex. It should be noted that there are two components of the 5f shell (and likewise for the 6d shell) that can engage in π -interactions with

the oxo ligand and the contributions reported in this paper are the composite of these two distinct interactions. Therefore, the degree of electron sharing is greater for the σ -component of each bond than for each of the π -components.

While there is an overall reduction in $\delta(U, O)$ upon completion, this reduction is not distributed evenly among the four bonding components. Taking the fluoride complex as an example, the $5f_{\sigma}$ contribution is largely unchanged and is reduced to 95% of its free value while the $5f_{\pi}$ contribution reduces to 72% of its free value. Corresponding $6d$ contributions reduce to 80% and 69%, respectively. This variation can be understood in terms of the availability of these shells to equatorial bonding interactions: the $5f_{\sigma}$ and $6d_{\sigma}$ components are orientated along the U-O bond and are, therefore, relatively unavailable for equatorial interactions while the $5f_{\pi}$ and $6d_{\pi}$ components are available for equatorial σ -bonding and π -bonding interactions, respectively, and are, therefore, most significantly affected by the presence of equatorial ligands. Qualitatively similar behavior is found for the other halide complexes.

More broadly, the quantitative difference in the reduction of ρ_{BCP} (which is only sensitive to σ -interactions) and the σ -contributions to $\delta(U, O)$ demonstrate how these metrics provide independent but related data regarding bonding. This is most obvious for the $5f$ -shell: the $5f$ contribution to ρ_{BCP} reduces to 71% of its free value upon equatorial coordination by fluoride while the corresponding $5f_{\sigma}$ contribution to $\delta(U, O)$ maintains 95% of its free value, i.e., overlap-induced covalency is reduced while degeneracy-induced covalency is maintained.

Figure 3 summarizes QTAIM metrics for equatorial U-X bonds in $[UO_2X_4]^{2-}$ and UX_6 complexes (see Supplementary Materials for numerical data). This data was obtained by taking a U-X bond to define the principal molecular axis and reference to σ -contributions and π -contributions to bonding is given in this study with respect to the U-X bond. This approach is taken throughout this contribution.

Considering first $\rho_{BCP}(U, X)$, overall magnitudes are larger in the UX_6 complexes due to the lack of competition with the strongly coordinating terminal oxo species and the consequently shorter U-X bonds. The $\rho_{BCP}(U, X)$ values are, however, much lower than those of the U-O bond, which indicates, as expected, significantly reduced covalent contributions to bonding. Nonetheless, $\rho_{BCP}(U, X)$ has a maximum value (0.155 a.u.) in UF_6 , consistent with substantial covalent bond character. There is a clear reduction in $\rho_{BCP}(U, X)$ in both sets of complexes as the halide mass increases, which shows a reduction in overlap-induced equatorial covalency. Interestingly, the reduction is significantly more pronounced for the $5f$ shell. The $5f$ contribution to ρ_{BCP} is 34% and 38% larger than the $6d$ contribution in $[UO_2F_4]^{2-}$ and UF_6 , respectively, but is just 4% and 7% larger in $[UO_2Br_4]^{2-}$ and UBr_6 , respectively. There is a larger contribution to bonding from the $5f$ shell in fluoride complexes while $5f$ and $6d$ contributions are comparable for the heavier halides.

The value of ρ_{BCP} in UF_6 can be indirectly compared to a recent X-ray diffraction study of $[UF_6]^{-}$ in which topological analysis of the experimentally determined electron density gave $\rho_{BCP} \sim 0.135$ a.u. for the U-F bond [21]. This is approximately 13% lower than the value reported here, but it should be borne in mind that uranium is in the +5 oxidation state in $[UF_6]^{-}$ as opposed to the +6 oxidation state in UF_6 . We have previously investigated the dependence of QTAIM parameters on uranium oxidation state in uranium hexachloride [61], finding a reduction in ρ_{BCP} of 17% when comparing the +6 and +5 oxidation states. These recent experimental findings, therefore, appear to be in accord with the present study, which suggests a significant decrease in the overlap-driven covalent bond character upon the reduction of the uranium center in both hexachloride and hexafluoride species.

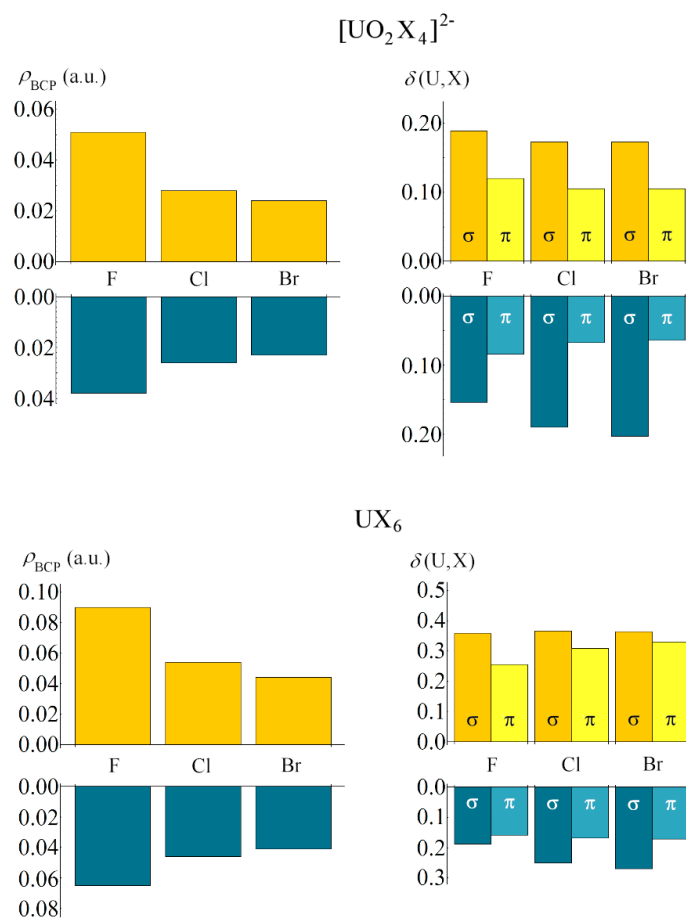


Figure 3. Decomposed QTAIM metrics of the U-X bond in $[\text{UO}_2\text{X}_4]^{2-}$ and UX_6 complexes ($\text{X} = \text{F}, \text{Cl}, \text{Br}$) obtained from B3LYP-derived densities. f-shell contributions are given in yellow and d-shell contributions are in blue.

Variation in $\delta(\text{U}, \text{X})$ is markedly different in the two sets of complexes. For UX_6 species, an overall increase is found as the halide mass increases, which opposes the trend in ρ_{BCP} and shows the danger of attempting to use δ as an indicator of bond order in the presence of bond polarization. 5f components of $\delta(\text{U}, \text{X})$ are consistently higher than 6d contributions with the 5f $_{\sigma}$ contribution dominating the fluoride complex and all components increasing as the halide mass increases. This behavior again opposes that exhibited by ρ_{BCP} and demonstrates that overlap-induced and degeneracy-induced covalency can (i) manifest independently and (ii) both be identified by the methodology employed here. For $[\text{UO}_2\text{X}_4]^{2-}$ species, the trend in 5f $_{\sigma}$, 5f $_{\pi}$, and 6d $_{\pi}$ components mirrors that of ρ_{BCP} while the variation in 6d $_{\sigma}$ strongly opposes this trend and results in the overall magnitude of $\delta(\text{U}, \text{X})$ remaining largely unchanged with the 6d $_{\sigma}$ component overtaking 5f $_{\sigma}$ as the dominant contribution when the halide mass increases. The qualitative difference in $\delta(\text{U}, \text{X})$ between the two sets of complexes presumably reflects the strong influence of the axial oxo species on (formally) uranium-based energy levels.

2.3. Heterohalide Complexes

In this section, complexes of the form $[\text{UO}_2\text{X}_2\text{Y}_2]^{2-}$ and $\text{UX}_2\text{Y}_2\text{Z}_2$ (where $\text{X}, \text{Y}, \text{Z} \in \{\text{F}, \text{Cl}, \text{Br}\}$) are considered. Again, these complexes possess D_{2h} symmetry or higher, which implies that like ligands are oriented *trans* to each other and allows for the equivalent analysis to that reported in Section 2.2 to be performed. In the case of the $\text{UX}_2\text{Y}_2\text{Z}_2$ complexes, only the “axial” U–X bond is considered

since the permutation of the ligands means that each of the bonding interactions in the 10 possible complexes is thus included.

Figure 4 summarizes calculated ρ_{BCP} values of the axial bond (numerical values are presented in the Supplementary Materials). Focusing initially on the uranyl halides, the characteristics identified in Section 2.2 are maintained, i.e., that equatorial ligand sets including the lighter, more electronegative halides perturb the axial U–O bond more with the 5f and 6d contributions being approximately equally affected. The effect of altering the equatorial ligand set in the uranium halides is less pronounced, presumably due to the more ionic nature of the interactions. ρ_{BCP} attains a maximum value 0.160 a.u. for the U–F bond with an equatorial ligand set comprised of Cl and/or Br. This is, however, just 3% larger than the value found in UF_6 . Broadly speaking, there is a modest perturbation to ρ_{BCP} when the equatorial ligand set includes F while calculated metrics are almost completely insensitive to replacing Cl by Br.

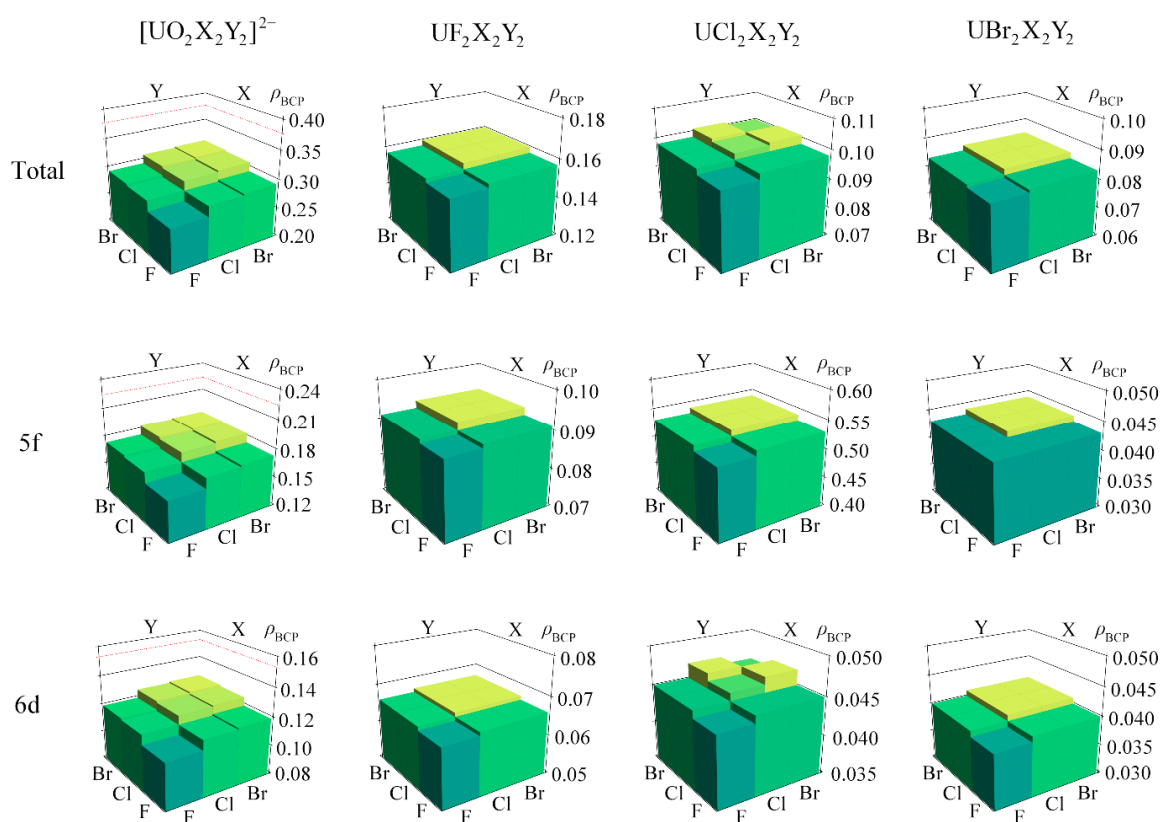


Figure 4. ρ_{BCP} values of axial U–O and U–X (X = F, Cl, Br) bonds in $[\text{UO}_2\text{X}_2\text{Y}_2]^{2-}$ and $\text{UX}_2\text{Y}_2\text{Z}_2$ complexes derived from B3LYP-generated densities. All values are in a.u.

Delocalization indices exhibit more variation (See Figure 5: numerical values presented in Supplementary Materials). $\delta(\text{U}, \text{O})$ exhibits the same variation as reported in Section 2.2 with larger values found when the halide mass increases. The $5f_\sigma$ contribution is, in all cases, close to the value for free uranyl and insensitive to the equatorial ligand set. Other contributions vary in accordance with the total value, with the $6d_\pi$ component exhibiting the greatest sensitivity. As previously discussed, this component of the 6d shell is also able to engage in equatorial π -bonding interactions and the variation seen here is indicative of the formation of such bonding interactions even though this should be interpreted in the context of degeneracy-driven covalency.

All $\text{UX}_2\text{Y}_2\text{Z}_2$ complexes exhibit qualitatively similar trends. Total values of $\delta(\text{U}, \text{X})$ are largely insensitive to the equatorial environment, which increases slightly as the equatorial ligands become heavier and less electronegative. A trend is also exhibited by the $5f_\pi$ and $6d_\sigma$ contributions.

The $5f_{\sigma}$ contribution decreases as the halide mass increases, but, in contrast, the $6d_{\pi}$ component increases by a greater magnitude. Since both the $5f_{\sigma}$ and $6d_{\pi}$ components are available for equatorial π -bonding interactions, the variation in $\delta(U, X)$ can, therefore, be attributed to increased equatorial π -interactions with the $6d$ shell, which is partially balanced by a reduction in such interactions with the $5f$ shell. This is indicative of closer energetic matching of fluorine $2p$ and uranium $5f$ levels and of bromine $4p$ and uranium $6d$ levels.

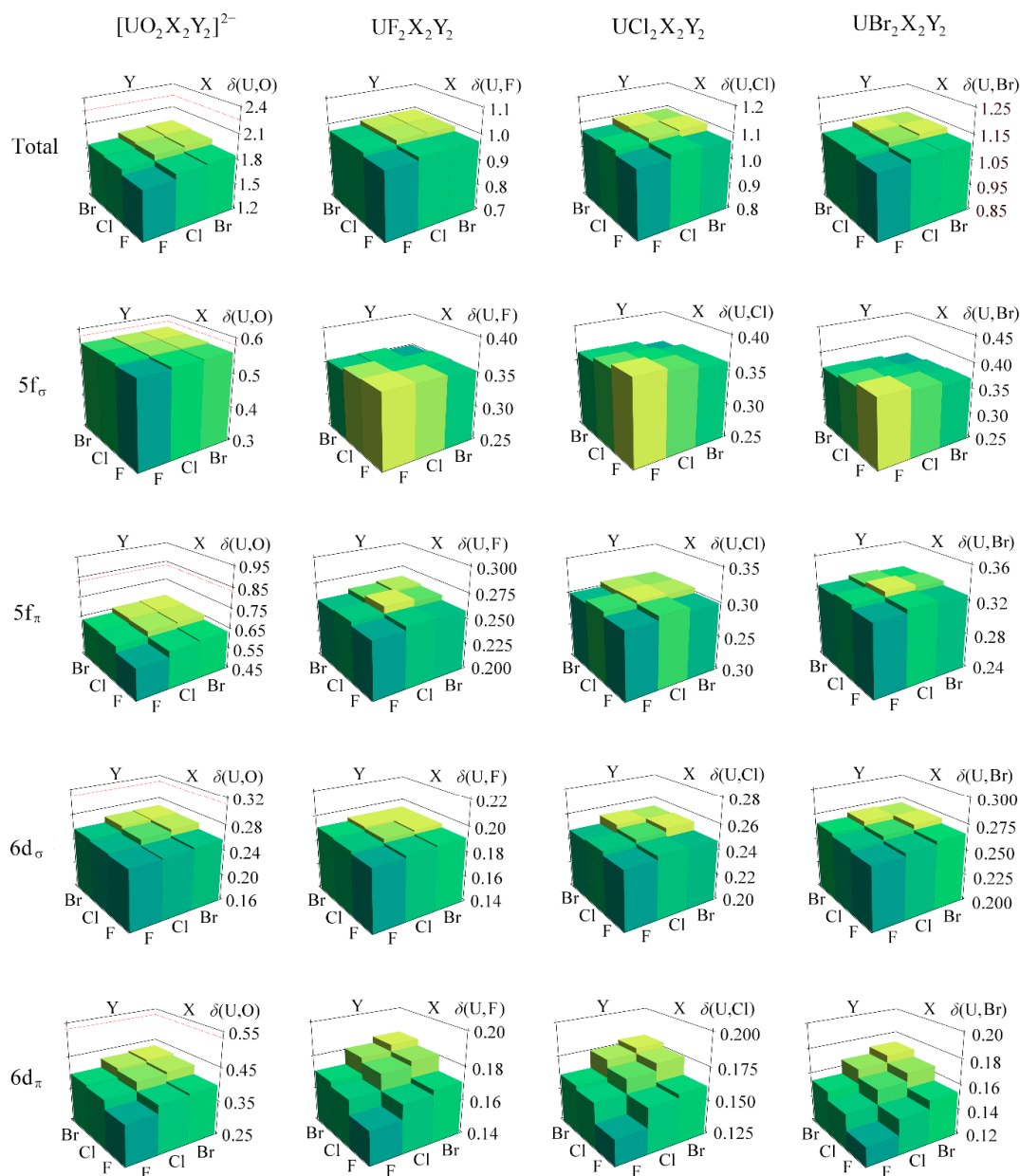


Figure 5. Delocalization indices of axial U–O and U–X (X = F, Cl, Br) bonds in $[\text{UO}_2\text{X}_2\text{Y}_2]^{2-}$ and $\text{UX}_2\text{Y}_2\text{Z}_2$ complexes derived from B3LYP-generated densities. All values are in a.u.

2.4. Covalency and Bond Stabilization

Lastly, the relationship between equatorial bond covalency and bond stability is considered. For uranyl, the binding energy of the equatorial ligand set is defined by the equation below.

$$E_B = E(\text{UO}_2^{2+}) + 2E(\text{X}^-) + 2E(\text{Y}^-) - E([\text{UO}_2\text{X}_2\text{Y}_2]^{2-}) \quad (3)$$

so that E_B is positive for a stabilizing interaction.

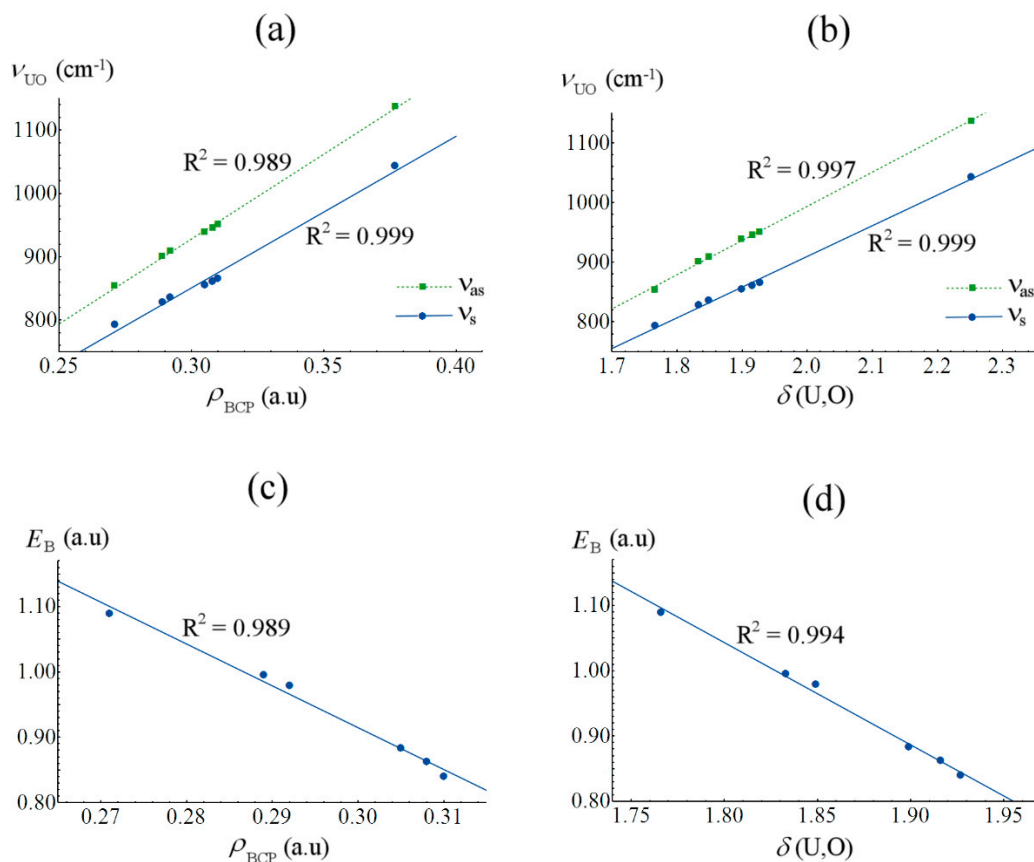


Figure 6. Correlation between QTAIM parameters of the U–O bond, U–O stretching vibrational frequencies, and the binding energy of the equatorial ligand set in $[\text{UO}_2\text{X}_2\text{Y}_2]^{2-}$ complexes. (a) correlates ν_{UO} and ρ_{BCP} , (b) correlates ν_{UO} and $\delta(\text{U,O})$, (c) correlates E_B and ρ_{BCP} , (d) correlates E_B and $\delta(\text{U,O})$.

Figure 6 reports correlations between QTAIM parameters of the UO bond, U–O stretching vibrational frequencies (ν_{UO}), and the binding energy (E_B) of the equatorial ligand set (see Supplementary Materials for numerical data). Extremely strong correlations are found between vibrational frequencies and both ρ_{BCP} and $\delta(\text{U,O})$ (Figures 6a and 6b, respectively), which indicates that the covalency of the U–O bond is strongly stabilizing. We have previously reported similar strong correlations with a more varied ligand set [75]. Perhaps more interestingly, strong anti-correlations are also found between these topological parameters and binding energies, which is defined in Equation (3). These anti-correlations (Figure 6c,d) illustrate the perturbation of the U–O bond covalency by the presence of the equatorial ligands, which suggests that U–O bond vibrations can be used as a quantitative probe of equatorial ligand stability.

It might be expected that binding energies would also correlate with QTAIM parameters of the axial bonds. Figure 7 summarizes these relationships (see Supplementary Materials for numerical data). Note that since both homoleptic and heteroleptic complexes are considered, averaged topological values are reported. We have taken this approach previously and found strong correlations between averaged values and binding energies [75].

Figure 7a illustrates an extremely strong correlation between $\bar{\rho}_{\text{BCP}}$ and E_B , which provides further justification for considering these averaged values. Conversely, no correlation is found between $\bar{\delta}$ and E_B (Figure 7b). This can be rationalized if one considers the aspects of covalency that ρ_{BCP} and $\bar{\delta}$ probe [57]: ρ_{BCP} identifies overlap-driven covalency, i.e., charge accumulation in the bonding region,

which might be expected to have a stabilizing effect on the interaction. δ , on the other hand, can be considered a measure of degeneracy-driven covalency for which no energetic stabilization of the bond is necessarily manifested. The absence of correlation presented in Figure 7b is, therefore, indicative of the fact that, in these complexes, degeneracy-driven covalency has no clearly-defined energetic effect. It should also be noted that variation in δ is rather modest with maximum deviations less than 2% from the mean value. In contrast, maximum ρ_{BCP} deviations are $\sim 40\%$ from the mean.

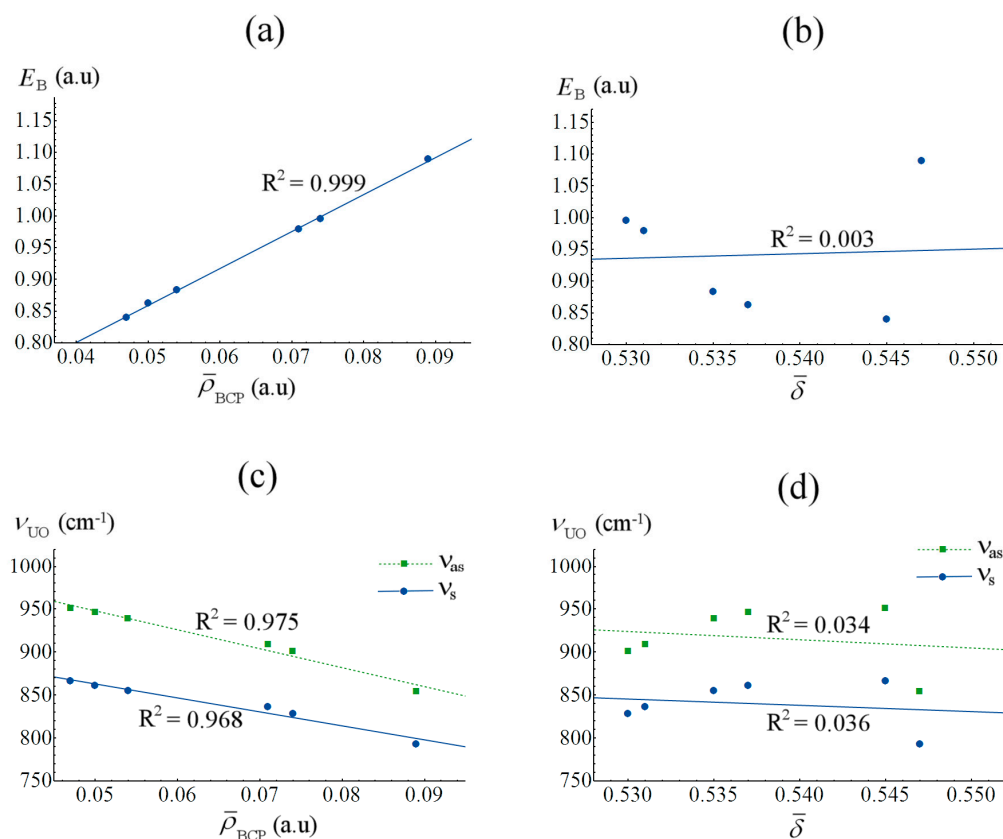


Figure 7. Correlation between QTAIM parameters of the equatorial bonds, the binding energy of the equatorial ligand set, and the U–O stretching vibrational frequencies in $[\text{UO}_2\text{X}_2\text{Y}_2]^{2-}$ complexes. (a) correlates E_B and $\bar{\rho}_{\text{BCP}}$, (b) correlates E_B and δ , (c) correlates ν_{UO} and $\bar{\rho}_{\text{BCP}}$, (d) correlates ν_{UO} and δ .

Since ν_{UO} correlated strongly with E_B and E_B itself correlated strongly with $\bar{\rho}_{\text{BCP}}$ for the equatorial bonds, the direct relationship between ν_{UO} and equatorial bond parameters was considered (see Figures 7c and 7d). As expected, a very strong (albeit slightly weaker) anticorrelation was found with $\bar{\rho}_{\text{BCP}}$ while correlation with δ was not identified. The anti-correlation with $\bar{\rho}_{\text{BCP}}$ lends further support to our previous assertion that ν_{UO} could be used to probe equatorial bond covalency [75].

The success of correlating the averaged equatorial ρ_{BCP} values with binding energies in uranyl halides suggested that a similar approach might be applicable to the uranium hexahalides considered in this study where the average would be with respect to all coordinating species. The binding energy is defined by the equation below.

$$E_B = E(\text{U}^{6+}) + 2E(\text{X}^-) + 2E(\text{Y}^-) + 2E(\text{Z}^-) - E(\text{UX}_2\text{Y}_2\text{Z}_2). \quad (4)$$

Figure 8 presents the results of correlating E_B with $\bar{\rho}_{\text{BCP}}$ and δ (See Supplementary Materials for numerical data). As seen for the uranyl halides, $\bar{\rho}_{\text{BCP}}$ exhibits an excellent correlation with E_B and again demonstrates that $\bar{\rho}_{\text{BCP}}$ quantitatively measures stabilizing covalent interactions in these species.

Remarkably, $\bar{\delta}$ shows a very strong anti-correlation with E_B , i.e., as degeneracy-driven covalency increases, bond stability reduces.

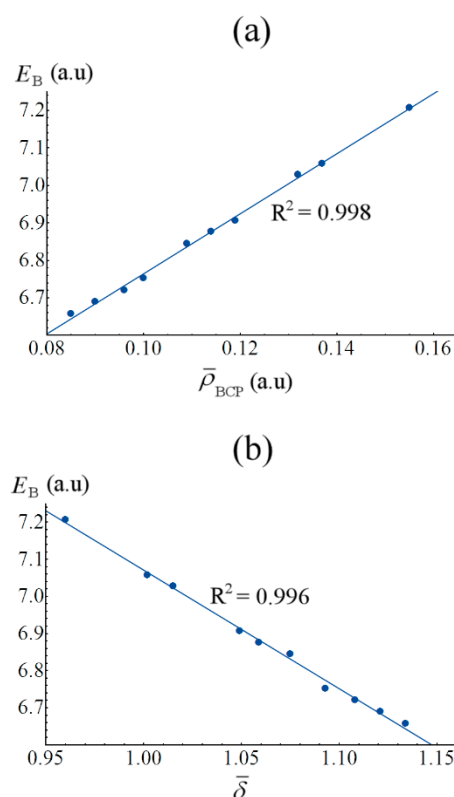


Figure 8. Correlation between the averaged QTAIM parameters of U–X, U–Y & U–Z bonds and the total binding energy in $UX_2Y_2Z_2$ complexes. (a) correlates E_B and $\bar{\rho}_{BCP}$, (b) correlates E_B and $\bar{\delta}$.

3. Computational Details

All calculations were performed using version 6.6 of the TURBOMOLE quantum chemistry code [82,83] using scalar-relativistic density functional theory (DFT). Several exchange-correlation (xc -) functionals were considered in order to identify which was most suitable for these simulations and, as reported above, the hybrid-GGA B3LYP functional [71,72] was found to give the best agreement with experimental data in test systems. There are numerous examples in the literature demonstrating the suitability of B3LYP in the study of U(VI) coordination complexes [34,37,75,78]. All simulations were performed using the Ahlrichs def2-QZVP basis sets [84] of polarized quadruple- ζ quality for light atoms (O, F, Cl, Br). The small-core pseudopotential of Dolg and co-workers [85], along with the corresponding (14s13p10d8f6g)/[10s9p5d4f3g] basis set [86], was used to model the uranium center by incorporating scalar relativistic effects. This pseudopotential is constructed from calculations employing the Wood-Boring equation (which may be derived directly from the Dirac equation) and includes both a mass-velocity and a Darwin term. The effects of the spin-orbit coupling have not been considered in these closed shell, formally $5f^06d^0$ species. De Jong et al. have shown that the effects of spin-orbit coupling are rather moderate in the high energy valence region of uranyl but become more pronounced when considering the pseudo core 6p-shell [87]. However, we have recently shown that the impact of the 6p-shell on QTAIM metrics is modest [88]. We would also expect the degree of SO-coupling to be comparable in analogous systems and, therefore, have little impact on the trends reported here.

Geometry optimizations were performed in the gas-phase using default convergence criteria and local energetic minima were identified using analytical frequency analysis. In order to decompose

bonding into contributions from different electronic shells, all optimizations were constrained to the D_{2h} point group. Topological and integrated properties of the electron density were evaluated using version 3.3.9 of the Multiwfn code [89].

4. Summary and Conclusions

The electronic structures of a series of uranium hexahalide and uranyl tetrahalide complexes were simulated at the density functional theoretical (DFT) level. A comparison with previous experimental structural and vibrational data indicated that the B3LYP exchange-correlation functional was best able to accurately simulate these complexes. B3LYP-derived electronic structures were subsequently analyzed using a novel application of the Quantum Theory of Atoms in Molecules (QTAIM). This approach exploited the high (D_{2h} or greater) symmetry of the complexes to determine 5f-shell and 6d-shell contributions to bonding through symmetry arguments. The analysis also allowed differentiation between overlap-driven and degeneracy-driven contributions to covalency and, for the latter, to further differentiate between σ -type and π -type interactions. This analysis revealed that, of the halogen ligands considered ($X = F, Cl, Br$), fluoride ligation resulted in the strongest bonds with the most significant covalent character and with values of the density at the U-F bond critical point, ρ_{BCP} , as high as 0.16 a.u. As a reference, $\rho_{BCP} \geq 0.20$ a.u. is often taken to be an indicator of a predominantly covalent interaction. Ligation by chloride and bromide species resulted in more ionic interactions with little differentiation between the ligands. Fluoride ligands were also found to be most capable of perturbing the electronic structure of other bonds in the complex. Taking $[UO_2F_4]^{2-}$ as an example, QTAIM metrics of the U–O bond were reduced to ~75% of the values for free uranyl.

The QTAIM analysis allows for the distinction to be made between covalent bond contributions whose origin lies in either orbital overlap or energy degeneracy. Analysis of the complexes considered here showed that 5f contributions to overlap-driven covalency were larger than 6d contributions for all interactions in all complexes studied while degeneracy-driven covalent contributions showed significantly greater variation. σ -contributions to degeneracy-driven covalency were found to be consistently larger than those of each individual π -component even though the total π -contribution was, in some cases, larger.

We have previously reported on strong correlations between uranyl stretching vibrational frequencies and equatorial bond covalency [75]. In this study, strong correlations were found between overlap-driven covalent bond contributions, U–O vibrational frequencies, and energetic stability, which indicates that overlap-driven covalency leads to bond stabilization in these complexes and that uranyl vibrational frequencies can be used to quantitatively probe equatorial bond covalency. For uranium hexahalides, overlap-driven covalency was shown to strongly correlate with bond stability while degeneracy-driven covalency was found to strongly anti-correlate. This anti-correlation illustrates the care that must be taken to differentiate between overlap-driven and degeneracy-driven covalent contributions to bond character when employing such analysis to rationalize experimental data. This work demonstrates that the QTAIM can be used to provide a highly detailed characterization of bonding interactions, which distinguishes between the different origins of covalent contributions and provides quantitative data with which to rationalize observable phenomena.

Supplementary Materials: The following are available online at <http://www.mdpi.com/2304-6740/6/3/88/s1>. Tables S1–S10: numerical data using which graphs and figures have been generated.

Author Contributions: Conceptualization, A.K. Methodology, A.K. Formal Analysis, J.T., M.L., and A.K. Writing-Original Draft Preparation, J.T., M.L., and A.K. Writing-Review & Editing, J.T., M.L., and A.K. Visualization, A.K. Supervision, A.K. Project Administration, A.K.

Funding: This research received no external funding.

Conflicts of Interest: The authors declare no conflict of interest.

References

1. Jensen, M.P.; Bond, A.H. Comparison of covalency in the complexes of trivalent actinide and lanthanide cations. *J. Am. Chem. Soc.* **2002**, *124*, 9870–9877. [[CrossRef](#)] [[PubMed](#)]
2. Gregson, M.; Lu, E.; Tuna, F.; McInnes, E.J.L.; Hennig, C.; Scheinost, A.C.; McMaster, J.; Lewis, W.; Blake, A.J.; Kerridge, A.; et al. Emergence of Comparable Covalency in Isostructural Cerium(IV)- and Uranium(IV)-Carbon Multiple Bonds. *Chem. Sci.* **2016**, *7*, 3286–3297. [[CrossRef](#)] [[PubMed](#)]
3. Gregson, M.; Lu, E.; Mills, D.; Tuna, F.; McInnes, E.; Hennig, C.; Scheinost, A.; McMaster, J.; Lewis, W.; Blake, A.; et al. The inverse-trans-influence in tetravalent lanthanide and actinide bis(carbene) complexes. *Nat. Commun.* **2017**, *8*, 14137. [[CrossRef](#)] [[PubMed](#)]
4. Kozimor, S.A.; Yang, P.; Batista, E.R.; Boland, K.S.; Burns, C.J.; Clark, D.L.; Conradson, S.D.; Martin, R.L.; Wilkerson, M.P.; Wolfsberg, L.E. Trends in covalency for d- and f-element metallocene dichlorides identified using chlorine K-edge X-ray absorption spectroscopy and time-dependent density functional theory. *J. Am. Chem. Soc.* **2009**, *131*, 12125–12136. [[CrossRef](#)] [[PubMed](#)]
5. Minasian, S.G.; Keith, J.M.; Batista, E.R.; Boland, K.S.; Clark, D.L.; Conradson, S.D.; Kozimor, S.A.; Martin, R.L.; Schwarz, D.E.; Shuh, D.K.; et al. Determining relative f and d orbital contributions to M–Cl covalency in MCl_6^{2-} (M = Ti, Zr, Hf, U) and $UOCl_5^-$ using Cl K-edge X-ray absorption spectroscopy and time-dependent density functional theory. *J. Am. Chem. Soc.* **2012**, *134*, 5586–5597. [[CrossRef](#)] [[PubMed](#)]
6. Spencer, L.P.; Yang, P.; Minasian, S.G.; Jilek, R.E.; Batista, E.R.; Boland, K.S.; Boncella, J.M.; Conradson, S.D.; Clark, D.L.; Hayton, T.W.; et al. Tetrahalide complexes of the $[U(NR)_2]^{2+}$ ion: Synthesis, theory, and chlorine K-edge X-ray absorption spectroscopy. *J. Am. Chem. Soc.* **2013**, *135*, 2279–2290. [[CrossRef](#)] [[PubMed](#)]
7. Minasian, S.G.; Keith, J.M.; Batista, E.R.; Boland, K.S.; Clark, D.L.; Kozimor, S.A.; Martin, R.L.; Shuh, D.K.; Tylliszczak, T. New evidence for 5f covalency in actinocenes determined from carbon K-edge XAS and electronic structure theory. *Chem. Sci.* **2014**, *5*, 351–359. [[CrossRef](#)]
8. Altman, A.B.; Pacold, J.I.; Wang, J.; Lukens, W.W.; Minasian, S.G. Evidence for 5d- σ and 5d- π covalency in lanthanide sesquioxides from oxygen K-edge X-ray absorption spectroscopy. *Dalt. Trans.* **2016**, *45*, 9948–9961. [[CrossRef](#)] [[PubMed](#)]
9. Löble, M.W.; Keith, J.M.; Altman, A.B.; Stieber, S.C.E.; Batista, E.R.; Boland, K.S.; Conradson, S.D.; Clark, D.L.; Lezama Pacheco, J.; Kozimor, S.A.; et al. Covalency in Lanthanides. An X-ray Absorption Spectroscopy and Density Functional Theory Study of $LnCl_6^{x-}$ (x = 3, 2). *J. Am. Chem. Soc.* **2015**, *137*, 2506–2523. [[CrossRef](#)] [[PubMed](#)]
10. Minasian, S.G.; Batista, E.R.; Booth, C.H.; Clark, D.L.; Keith, J.M.; Kozimor, S.A.; Lukens, W.W.; Martin, R.L.; Shuh, D.K.; Stieber, S.C.E.; et al. Quantitative Evidence for Lanthanide-Oxygen Orbital Mixing in CeO_2 , PrO_2 , and TbO_2 . *J. Am. Chem. Soc.* **2017**, *139*, 18052–18064. [[CrossRef](#)] [[PubMed](#)]
11. Dumas, T.; Guillaumont, D.; Fillaux, C.; Scheinost, A.; Moisy, P.; Petit, S.; Shuh, D.K.; Tylliszczak, T.; Auwer, C. Den. The nature of chemical bonding in actinide and lanthanide ferrocyanides determined by X-ray absorption spectroscopy and density functional theory. *Phys. Chem. Chem. Phys.* **2016**, *18*, 2887–2895. [[CrossRef](#)] [[PubMed](#)]
12. Formanuk, A.; Ariciu, A.M.; Ortu, F.; Beekmeyer, R.; Kerridge, A.; Tuna, F.; McInnes, E.J.L.; Mills, D.P. Actinide covalency measured by pulsed electron paramagnetic resonance spectroscopy. *Nat. Chem.* **2017**, *9*, 578–583. [[CrossRef](#)] [[PubMed](#)]
13. Seaman, L.A.; Wu, G.; Edelstein, N.; Lukens, W.W.; Magnani, N.; Hayton, T.W. Probing the 5f orbital contribution to the bonding in a U(V) ketimide complex. *J. Am. Chem. Soc.* **2012**, *134*, 4931–4940. [[CrossRef](#)] [[PubMed](#)]
14. Lukens, W.W.; Edelstein, N.M.; Magnani, N.; Hayton, T.W.; Fortier, S.; Seaman, L.A. Quantifying the σ and π interactions between U(V) f orbitals and halide, alkyl, alkoxide, amide and ketimide ligands. *J. Am. Chem. Soc.* **2013**, *135*, 10742–10754. [[CrossRef](#)] [[PubMed](#)]
15. Lukens, W.W.; Speldrich, M.; Yang, P.; Duignan, T.J.; Autschbach, J.; Kögerler, P. The roles of 4f- and 5f-orbitals in bonding: A magnetochemical, crystal field, density functional theory, and multi-reference wavefunctional study. *Dalt. Trans.* **2016**, 11508–11521. [[CrossRef](#)] [[PubMed](#)]
16. Smiles, D.E.; Wu, G.; Hrobárik, P.; Hayton, T.W. Use of ^{77}Se and ^{125}Te NMR Spectroscopy to Probe Covalency of the Actinide-Chalcogen Bonding in $[Th(E)_n]\{N(SiMe_3)_2\}_3^-$ (E = Se, Te; n = 1, 2) and Their Oxo-Uranium(VI) Congeners. *J. Am. Chem. Soc.* **2016**, *138*, 814–825. [[CrossRef](#)] [[PubMed](#)]

17. Adam, C.; Kaden, P.; Beele, B.B.; Müllich, U.; Trumm, S.; Geist, A.; Panak, P.J.; Denecke, M.A. Evidence for covalence in a N-donor complex of americium(III). *Dalton Trans.* **2013**, *42*, 14068–14074. [[CrossRef](#)] [[PubMed](#)]
18. Polinski, M.J.; Garner, E.B.; Maurice, R.; Planas, N.; Stritzinger, J.T.; Parker, T.G.; Cross, J.N.; Green, T.D.; Alekseev, E.V.; Van Cleve, S.M.; et al. Unusual structure, bonding and properties in a californium borate. *Nat. Chem.* **2014**, *6*, 387–392. [[CrossRef](#)] [[PubMed](#)]
19. Cary, S.K.; Vasiliu, M.; Baumbach, R.E.; Stritzinger, J.T.; Green, T.D.; Diefenbach, K.; Cross, J.N.; Knappenberger, K.L.; Liu, G.; Silver, M.A.; et al. Emergence of californium as the second transitional element in the actinide series. *Nat. Commun.* **2015**, *6*, 6827. [[CrossRef](#)] [[PubMed](#)]
20. Su, J.; Dau, P.D.; Liu, H.T.; Huang, D.L.; Wei, F.; Schwarz, W.H.E.; Li, J.; Wang, L.S. Photoelectron spectroscopy and theoretical studies of gaseous uranium hexachlorides in different oxidation states: UCl_6^{q-} ($q = 0-2$). *J. Chem. Phys.* **2015**, *142*, 134308. [[CrossRef](#)] [[PubMed](#)]
21. Gianopoulos, C.G.; Zhurov, V.V.; Minasian, S.G.; Batista, E.R.; Jelsch, C.; Pinkerton, A.A. Bonding in Uranium(V) Hexafluoride Based on the Experimental Electron Density Distribution Measured at 20 K. *Inorg. Chem.* **2017**, *56*, 1775–1778. [[CrossRef](#)] [[PubMed](#)]
22. Arnold, P.L.; Turner, Z.R.; Kaltsoyannis, N.; Pelekanaki, P.; Bellabarba, R.M.; Tooze, R.P. Covalency in Ce^{IV} and U^{IV} halide and N-heterocyclic carbene bonds. *Chem. Eur. J.* **2010**, *16*, 9623–9629. [[CrossRef](#)] [[PubMed](#)]
23. King, D.M.; Tuna, F.; McInnes, E.J.L.; McMaster, J.; Lewis, W.; Blake, A.J.; Liddle, S.T. Isolation and characterization of a uranium(VI)–nitride triple bond. *Nat. Chem.* **2013**, *5*, 482–488. [[CrossRef](#)] [[PubMed](#)]
24. Brown, J.L.; Fortier, S.; Wu, G.; Kaltsoyannis, N.; Hayton, T.W. Synthesis and Spectroscopic and Computational Characterization of the Chalcogenido-Substituted Analogues of the Uranyl Ion, $[OUE]^{2+}$ ($E = S, Se$). *J. Am. Chem. Soc.* **2013**, *135*, 5352–5355. [[CrossRef](#)] [[PubMed](#)]
25. Arliguie, T.; Belkhir, L.; Bouaoud, S.; Thuery, P.; Villiers, C.; Boucekkine, A.; Ephritikhine, M. Lanthanide(III) and Actinide(III) Complexes $[M(BH_4)_2(THF)_5][BPh_4]$ and $[M(BH_4)_2(18-crown-6)][BPh_4]$ ($M = Nd, Ce, U$): Synthesis, Crystal Structure, and Density Functional Theory Investigation of the Covalent Contribution to Metal-Borohydride Bonding. *Inorg. Chem.* **2009**, *48*, 221–230. [[CrossRef](#)] [[PubMed](#)]
26. Jones, M.B.; Gaunt, A.J.; Gordon, J.C.; Kaltsoyannis, N.; Neu, M.P.; Scott, B.L. Uncovering f-element bonding differences and electronic structure in a series of 1:3 and 1:4 complexes with a diselenophosphinate ligand. *Chem. Sci.* **2013**, *4*, 1189–1203. [[CrossRef](#)]
27. Gregson, M.; Wooles, A.J.; Cooper, O.J.; Liddle, S.T. Covalent Uranium Carbene Chemistry. *Comments Inorg. Chem.* **2015**, *35*, 262–294. [[CrossRef](#)]
28. Walensky, J.R.; Martin, R.L.; Ziller, J.W.; Evans, W.J. Importance of energy level matching for bonding in Th^{3+} - Am^{3+} actinide metallocene amidinates, $(C_5Me_5)_2[{}^iPrNC(Me)N^iPr]An$. *Inorg. Chem.* **2010**, *49*, 10007–10012. [[CrossRef](#)] [[PubMed](#)]
29. Behrle, A.C.; Barnes, C.L.; Kaltsoyannis, N.; Walensky, J.R. Systematic investigation of thorium(IV)- and uranium(IV)-ligand bonding in dithiophosphonate, thioselenophosphinate, and diselenophosphonate complexes. *Inorg. Chem.* **2013**, *52*, 10623–10631. [[CrossRef](#)] [[PubMed](#)]
30. Behrle, A.C.; Kerridge, A.; Walensky, J.R. Dithio- and Diselenophosphinate Thorium(IV) and Uranium(IV) Complexes: Molecular and Electronic Structures, Spectroscopy, and Transmetalation Reactivity. *Inorg. Chem.* **2015**, *54*, 11625–11636. [[CrossRef](#)] [[PubMed](#)]
31. Kaltsoyannis, N. Does covalency increase or decrease across the actinide series? Implications for minor actinide partitioning. *Inorg. Chem.* **2013**, *52*, 3407–3413. [[CrossRef](#)] [[PubMed](#)]
32. Tassell, M.J.; Kaltsoyannis, N. Covalency in $AnCp_4$ ($An = Th-Cm$): A comparison of molecular orbital, natural population and atoms-in-molecules analyses. *Dalt. Trans.* **2010**, *39*, 6719–6725. [[CrossRef](#)] [[PubMed](#)]
33. Kirker, I.; Kaltsoyannis, N. Does covalency really increase across the 5f series? A comparison of molecular orbital, natural population, spin and electron density analyses of $AnCp_3$ ($An = Th-Cm$; $Cp = \eta^5-C_5H_5$). *Dalton Trans.* **2011**, *40*, 124–131. [[CrossRef](#)] [[PubMed](#)]
34. Huang, Q.R.; Kingham, J.R.; Kaltsoyannis, N. The strength of actinide–element bonds from the quantum theory of atoms-in-molecules. *Dalt. Trans.* **2015**, *44*, 2554–2566. [[CrossRef](#)] [[PubMed](#)]
35. Trumm, M.; Schimmelpfennig, B.; Geist, A. Structure and separation quality of various N- and O-donor ligands from quantum-chemical calculations. *Nukleonika* **2015**, *60*, 847–851. [[CrossRef](#)]
36. Trumm, M.; Schimmelpfennig, B. Towards the origin of effective An(III)/Ln(III) separation by tridentate N-donor ligands: A theoretical study on atomic charges and polarisabilities for Cm(III)/Gd(III) separation. *Mol. Phys.* **2016**, *114*, 876–883. [[CrossRef](#)]

37. Vallet, V.; Wahlgren, U.; Grenthe, I. Probing the nature of chemical bonding in uranyl(VI) complexes with quantum chemical methods. *J. Phys. Chem. A* **2012**, *116*, 12373–12380. [[CrossRef](#)] [[PubMed](#)]
38. Szabo, Z.; Toraiishi, T.; Vallet, V.; Grenthe, I. Solution coordination chemistry of actinides: Thermodynamics, structure and reaction mechanisms. *Coord. Chem. Rev.* **2006**, *250*, 784–815. [[CrossRef](#)]
39. Di Pietro, P.; Kerridge, A. Assessing covalency in equatorial U–N bonds: Density based measures of bonding in BTP and isoamethyrin complexes of uranyl. *Phys. Chem. Chem. Phys.* **2016**, *18*, 16830–16839. [[CrossRef](#)] [[PubMed](#)]
40. Di Pietro, P.; Kerridge, A. Ligand size dependence of U–N and U–O bond character in a series of uranyl hexaphyrin complexes: Quantum chemical simulation and density based analysis. *Phys. Chem. Chem. Phys.* **2017**, *19*, 7546–7559. [[CrossRef](#)] [[PubMed](#)]
41. Fryer-Kanssen, I.; Austin, J.; Kerridge, A. Topological Study of Bonding in Aquo and Bis(triazinyl)pyridine Complexes of Trivalent Lanthanides and Actinides: Does Covalency Imply Stability? *Inorg. Chem.* **2016**, *55*, 10034–10042. [[CrossRef](#)] [[PubMed](#)]
42. Woodall, S.D.; Swinburne, A.N.; Kerridge, A.; Di Pietro, P.; Adam, C.; Kaden, P.; Natrajan, L.S. Neptunyl(VI) centred visible LMCT emission directly observable in the presence of uranyl(VI). *Chem. Commun.* **2015**, *51*, 5402–5405. [[CrossRef](#)] [[PubMed](#)]
43. Guillaumont, D. Quantum Chemistry Study of Actinide(III) and Lanthanide(III) Complexes with Tridentate Nitrogen Ligands. *J. Phys. Chem. A* **2004**, *108*, 6893–6900. [[CrossRef](#)]
44. Petit, L.; Joubert, L.; Maldivi, P.; Adamo, C. A comprehensive theoretical view of the bonding in actinide molecular complexes. *J. Am. Chem. Soc.* **2006**, *128*, 2190–2191. [[CrossRef](#)] [[PubMed](#)]
45. Petit, L.; Adamo, C.; Maldivi, P. Toward a Clear-Cut Vision on the Origin of Insights from Theory. *Society* **2006**, *45*, 8517–8522.
46. Lan, J.; Shi, W.; Yuan, L.; Zhao, Y.; Li, J.; Chai, Z. Trivalent Actinide and Lanthanide Separations by Tetradentate Nitrogen Ligands: A Quantum Chemistry Study. *Inorg. Chem.* **2011**, *50*, 9230–9237. [[CrossRef](#)] [[PubMed](#)]
47. Roy, L.E.; Bridges, N.J.; Martin, L.R. Theoretical insights into covalency driven f element separations. *Dalton Trans.* **2013**, *42*, 2636–2642. [[CrossRef](#)] [[PubMed](#)]
48. Dolg, M.; Cao, X.; Ciupka, J. Misleading evidence for covalent bonding from EuIII and AmIII density functional theory bond lengths. *J. Electron Spectros. Relat. Phenomena* **2014**, *194*, 8–13. [[CrossRef](#)]
49. Wang, C.; Cheng, C.; Su, J.; Huai, P. Bonding nature of the actinide tetrafluorides AnF₄ (An = Th–Cm). *Mol. Phys.* **2015**, *113*, 3450–3458. [[CrossRef](#)]
50. Kaneko, M.; Miyashita, S.; Nakashima, S. Bonding Study on the Chemical Separation of Am(III) from Eu(III) by S-, N-, and O-Donor Ligands by Means of All-Electron ZORA-DFT Calculation. *Inorg. Chem.* **2015**, *54*, 7103–7109. [[CrossRef](#)] [[PubMed](#)]
51. Bryantsev, V.S.; Hay, B.P. Theoretical prediction of Am(III)/Eu(III) selectivity to aid the design of actinide-lanthanide separation agents. *Dalt. Trans.* **2015**, 7935–7942. [[CrossRef](#)] [[PubMed](#)]
52. Duignan, T.; Autschbach, J. Impact of the Kohn-Sham Delocalization Error on the 4f Shell Localization and Population in Lanthanide Complexes. *J. Chem. Theory Comput.* **2016**, *12*, 3109–3121. [[CrossRef](#)] [[PubMed](#)]
53. Hu, S.X.; Li, W.L.; Dong, L.; Gibson, J.K.; Li, J. Crown ether complexes of actinyls: A computational assessment of AnO₂ (15-crown-5)²⁺ (An = U, Np, Pu, Am, Cm). *Dalt. Trans.* **2017**, *46*, 12354–12363. [[CrossRef](#)] [[PubMed](#)]
54. Madic, C.; Hudson, M.J.; Liljenzin, J.O.; Glatz, J.P.; Nannicini, R.; Facchini, A.; Kolarik, Z.; Odoj, R. Recent achievements in the development of partitioning processes of minor actinides from nuclear wastes obtained in the frame of the NEWPART European Programme (1996–1999). *Prog. Nucl. Energy* **2002**, *40*, 523–526. [[CrossRef](#)]
55. Nilsson, M.; Nash, K.L. Review article: A review of the development and operational characteristics of the TALSPEAK process. *Solvent Extr. Ion Exch.* **2007**, *25*, 665–701. [[CrossRef](#)]
56. Bader, R.F.W. *Atoms in Molecules: A Quantum Theory*; Oxford University Press: Oxford, UK, 1990.
57. Kerridge, A. Quantification of f-element covalency through analysis of the electron density: Insights from simulation. *Chem. Commun.* **2017**, *53*, 6685–6695. [[CrossRef](#)] [[PubMed](#)]
58. Zhurov, V.V.; Zhurova, E.A.; Stash, A.I.; Pinkerton, A.A. Characterization of bonding in cesium uranyl chloride: Topological analysis of the experimental charge density. *J. Phys. Chem. A* **2011**, *115*, 13016–13023. [[CrossRef](#)] [[PubMed](#)]
59. Kerridge, A. Oxidation state and covalency in f-element metallocenes (M = Ce, Th, Pu): A combined CASSCF and topological study. *Dalton Trans.* **2013**, *42*, 16428–16436. [[CrossRef](#)] [[PubMed](#)]

60. Kerridge, A. f-orbital covalency in the actinocenes (An = Th–Cm): Multiconfigurational studies and topological analysis. *RSC Adv.* **2014**, *4*, 12078–12086. [[CrossRef](#)]
61. Beekmeyer, R.; Kerridge, A. Assessing Covalency in Cerium and Uranium Hexachlorides: A Correlated Wavefunction and Density Functional Theory Study. *Inorganics* **2015**, *3*, 482–499. [[CrossRef](#)]
62. Dau, P.D.; Su, J.; Liu, H.T.; Liu, J.B.; Huang, D.L.; Li, J.; Wang, L.S. Observation and investigation of the uranyl tetrafluoride dianion (UO₂F₄²⁻) and its solvation complexes with water and acetonitrile. *Chem. Sci.* **2012**, *3*, 1137–1146. [[CrossRef](#)]
63. Van den Bossche, G.; Spirlet, M.R.; Rebizant, J. Structure of Diammonium Tetrabromodioxouranate(VI) Dihydrate. *Acta Crystallogr. C* **1987**, *43*, 383–384. [[CrossRef](#)]
64. Kimura, M.; Schomaker, V.; Smith, D.W.; Weinstock, B. Electron-Diffraction Investigation of the Hexafluorides of Tungsten, Osmium, Iridium, Uranium, Neptunium, and Plutonium. *J. Chem. Phys.* **1968**, *48*, 4001–4012. [[CrossRef](#)]
65. Mcdowell, R.S.; Asprey, L.B.; Paine, R.T. Vibrational spectrum and force field of uranium hexafluoride. *J. Chem. Phys.* **1974**, *61*, 3571–3580. [[CrossRef](#)]
66. Zachariasen, W.H. Crystal chemical studies of the 5f-series of elements. V. The crystal structure of uranium hexachloride. *Acta Crystallogr.* **1948**, *1*, 285–287. [[CrossRef](#)]
67. Perdew, J.; Burke, K.; Ernzerhof, M. Generalized Gradient Approximation Made Simple. *Phys. Rev. Lett.* **1996**, *77*, 3865–3868. [[CrossRef](#)] [[PubMed](#)]
68. Becke, A.D. Density-functional exchange-energy approximation with correct asymptotic behavior. *Phys. Rev. A* **1988**, *38*, 3098–3100. [[CrossRef](#)]
69. Lee, C.; Yang, W.; Parr, R.G. Development of the Colle-Salvetti correlation-energy formula into a functional of the electron density. *Phys. Rev. B* **1988**, *37*, 785–789. [[CrossRef](#)]
70. Adamo, C.; Barone, V. Toward reliable density functional methods without adjustable parameters: The PBE0 model. *J. Chem. Phys.* **1999**, *110*, 6158–6170. [[CrossRef](#)]
71. Becke, A.D. Density-functional thermochemistry. III. The role of exact exchange. *J. Chem. Phys.* **1993**, *98*, 5648. [[CrossRef](#)]
72. Stephens, P.; Devlin, F.; Chabalowski, C.; Frisch, M. Ab initio calculation of vibrational absorption and circular dichroism spectra using density functional force fields. *J. Phys. Chem.* **1994**, *98*, 11623–11627. [[CrossRef](#)]
73. Becke, A.D. A new mixing of Hartree–Fock and local density-functional theories. *J. Chem. Phys.* **1993**, *98*, 1372–1377. [[CrossRef](#)]
74. Bauzá, A.; Quiñero, D.; Deyà, P.M.; Frontera, A. Is the use of diffuse functions essential for the proper description of noncovalent interactions involving anions? *J. Phys. Chem. A* **2013**, *117*, 2651–2655. [[CrossRef](#)] [[PubMed](#)]
75. Di Pietro, P.; Kerridge, A. U-Oyl Stretching Vibrations as a Quantitative Measure of the Equatorial Bond Covalency in Uranyl Complexes: A Quantum-Chemical Investigation. *Inorg. Chem.* **2016**, *55*, 573–583. [[CrossRef](#)] [[PubMed](#)]
76. Watkin, D.J.; Denning, R.G.; Prout, K. Structure of dicaesium tetrachlorodioxouranium(VI). *Acta Crystallogr. Sect. C Cryst. Struct. Commun.* **1991**, *47*, 2517–2519. [[CrossRef](#)]
77. Bullock, J.I. Raman and infrared spectroscopic studies of the uranyl ion: The symmetric stretching frequency, force constants, and bond lengths. *J. Chem. Soc. A* **1969**, 781–784. [[CrossRef](#)]
78. Schreckenbach, G.; Hay, P.J.; Martin, R.L. Density functional calculations on actinide compounds: Survey of recent progress and application to [UO₂X₄]²⁻ (X = F, Cl, OH) and AnF₆ (An = U, Np, Pu). *J. Comput. Chem.* **1999**, *20*, 70–90. [[CrossRef](#)]
79. Batista, E.R.; Martin, R.L.; Hay, P.J. Density functional investigations of the properties and thermochemistry of UF_n and UCl_n (n = 1, ..., 6). *J. Chem. Phys.* **2004**, *121*, 11104–11111. [[CrossRef](#)] [[PubMed](#)]
80. Grenthe, I.; Drozdzyński, J.; Fujino, T.; Buck, E.C.; Albrecht-Schmitt, T.E.; Wolf, S.F. Uranium. In *The Chemistry of the Actinide and Transactinide Elements*; Morss, L.R., Edelstein, N.M., Fuger, J., Katz, J.J., Eds.; Springer: Dordrecht, The Netherlands, 2006; pp. 253–698.
81. Yun-guang, Z.; Yu-de, L. Relativistic density functional investigation of UX₆ (X = F, Cl, Br and I). *Chin. Phys. B* **2010**, *19*, 033302. [[CrossRef](#)]
82. TURBOMOLE, version 6.6, A development of University of Karlsruhe and Forschungszentrum Karlsruhe GmbH. 2014. Available online: <http://www.turbomole.com> (accessed on 29 August 2018).

83. Ahlrichs, R.; Bär, M.; Häser, M.; Horn, H.; Kölmel, C. Electronic structure calculations on workstation computers: The program system turbomole. *Chem. Phys. Lett.* **1989**, *162*, 165–169. [[CrossRef](#)]
84. Weigend, F.; Ahlrichs, R. Balanced basis sets of split valence, triple zeta valence and quadruple zeta valence quality for H to Rn: Design and assessment of accuracy. *Phys. Chem. Chem. Phys.* **2005**, *7*, 3297–3305. [[CrossRef](#)] [[PubMed](#)]
85. Küchle, W.; Dolg, M.; Stoll, H.; Preuss, H. Energy-adjusted pseudopotentials for the actinides. Parameter sets and test calculations for thorium and thorium monoxide. *J. Chem. Phys.* **1994**, *100*, 7535–7542. [[CrossRef](#)]
86. Cao, X.; Dolg, M. Segmented contraction scheme for small-core actinide pseudopotential basis sets. *J. Mol. Struct. THEOCHEM* **2004**, *673*, 203–209. [[CrossRef](#)]
87. De Jong, W.A.; Visscher, L.; Nieuwpoort, W.C. On the bonding and the electric field gradient of the uranyl ion. *J. Mol. Struct.* **1999**, *458*, 41–52. [[CrossRef](#)]
88. Fryer-Kanssen, I.; Kerridge, A. Elucidation of the inverse trans influence in uranyl, its imido and carbene analogues via quantum chemical simulation. *Chem. Commun.* **2018**, *54*, 9761–9764. [[CrossRef](#)] [[PubMed](#)]
89. Lu, T.; Chen, F. Multiwfn: A multifunctional wavefunction analyzer. *J. Comput. Chem.* **2012**, *33*, 580–592. [[CrossRef](#)] [[PubMed](#)]



© 2018 by the authors. Licensee MDPI, Basel, Switzerland. This article is an open access article distributed under the terms and conditions of the Creative Commons Attribution (CC BY) license (<http://creativecommons.org/licenses/by/4.0/>).